A&A 407, 925–934 (2003)
DOI: 10.1051/0004-6361:20030910

Astronomy & Astrophysics

An *XMM-Newton* observation of the very young open cluster NGC 6383⋆,⋆⋆

G. Rauw[1,⋆⋆⋆], M. De Becker[1], E. Gosset[1,⋆⋆⋆], J. M. Pittard[2], and I. R. Stevens[3]

[1] Institut d'Astrophysique, Université de Liège, Allée du 6 Août, Bât. B5c, 4000 Liège (Sart Tilman), Belgium
[2] Department of Physics & Astronomy, University of Leeds, Leeds LS2 9JT, UK
[3] School of Physics & Astronomy, University of Birmingham, Edgbaston Birmingham B15 2TT, UK

Received 13 February 2003 / Accepted 16 June 2003

Abstract. We report the detection of a number of X-ray sources associated with the very young open cluster NGC 6383. About two thirds of these objects are correlated with a rather faint optical source and all but one have at least one infrared counterpart within a correlation radius of 8 arcsec. Although NGC 6383 is not associated with a prominent star forming region, the overall properties of many of the X-ray sources suggest that they may be candidates for low-mass pre-main sequence stars. The number of X-ray sources increases towards the cluster center suggesting that there exists a close relation between the massive O-star binary system HD 159 176 in the cluster core and the population of X-ray bright low-mass objects in NGC 6383.

Key words. stars: pre-main sequence – X-rays: stars – open clusters and associations: individual: NGC 6383 – stars: early-type

1. Introduction

NGC 6383 is a relatively small young open cluster centered on the massive binary HD 159 176 (O7 V + O7 V). The fundamental properties of NGC 6383 (age, distance, ...) are still somewhat controversial. FitzGerald et al. (1978) derived a reddening of $E(B-V) = 0.33 \pm 0.02$, a distance of 1.5 kpc and an age of 1.7 Myr. On the other hand, Lloyd Evans (1978) inferred a smaller distance of 1.3 kpc and an upper limit on the cluster age of 4–5 Myr.

Unlike many young stellar clusters, NGC 6383 is not embedded in a bright emission nebula harboring large amounts of dust. However, a weak nebula S 11 (Sharpless 1953) of 1 degree radius is centered on HD 159 176 and the cluster lies right in front of the dense dust clouds that divide the Milky Way at this galactic latitude (Lloyd Evans 1978). Although the cluster is not associated with a prominent star-forming region, there is evidence for ongoing star formation in the cluster core. Eggen (1961) presented *UBV* photometry of 27 stars in NGC 6383. He pointed out that the cluster displays a normal main sequence to about spectral type A0 while redder stars fall above the main sequence in the $(B-V, V)$ colour-magnitude diagram. Eggen predicted that if T Tauri variables were present in NGC 6383, they should be found at $V \sim 14.6$. FitzGerald et al. (1978) identified eight probable pre-main sequence (PMS) stars. Lloyd Evans (1978) identified six variable stars that might be in a PMS evolutionary stage. Observations by Thé et al. (1985) and van den Ancker et al. (2000) revealed an infrared excess in the spectra of several cluster members. These excesses are most probably produced by thermal emission from circumstellar dust grains. However, unlike the situation in other young open clusters (see e.g. NGC 6530, Sung et al. 2000), a very deep survey for Hα emission is lacking for NGC 6383. Thé (1965) examined Hα photographic plates that went as deep as $V \sim 16.0$, but he failed to detect faint Hα emission stars. So far, only one Hα emitting object was reported in this cluster (van den Ancker et al. 2000). These authors suggested that this star might be a Herbig Ae/Be object.

In the present paper, we report the results of an *XMM-Newton* observation of NGC 6383. A detailed discussion of the X-ray spectrum of HD 159 176 is presented by De Becker et al. (2003). HD 159 176 and NGC 6383 were already detected in X-rays during the *ASCA* galactic plane survey with a GIS count rate of 0.060 cts s^{-1} in the 0.7–10 keV energy band (Sugizaki et al. 2001). However, our *XMM-Newton* observations have a far better spatial resolution and sensitivity and allow us therefore to perform a detailed investigation of the population of X-ray sources in the cluster. Since low and intermediate mass pre-main sequence stars are known to be prominent X-ray sources (see e.g. Neuhäuser 1997), we can take advantage of our data to investigate the star formation process in NGC 6383.

In Sect. 2, we discuss the detection of X-ray sources in NGC 6383, we summarize their X-ray properties and cross-correlate their positions with various catalogues in Sects. 2.1

Send offprint requests to: G. Rauw, e-mail: rauw@astro.ulg.ac.be

⋆ Based on observations with *XMM-Newton*, an ESA science mission with instruments and contributions directly funded by ESA member states and the USA (NASA).

⋆⋆ Table 1 is only available in electronic form at http://www.edpsciences.org

⋆⋆⋆ Research Associate FNRS (Belgium).

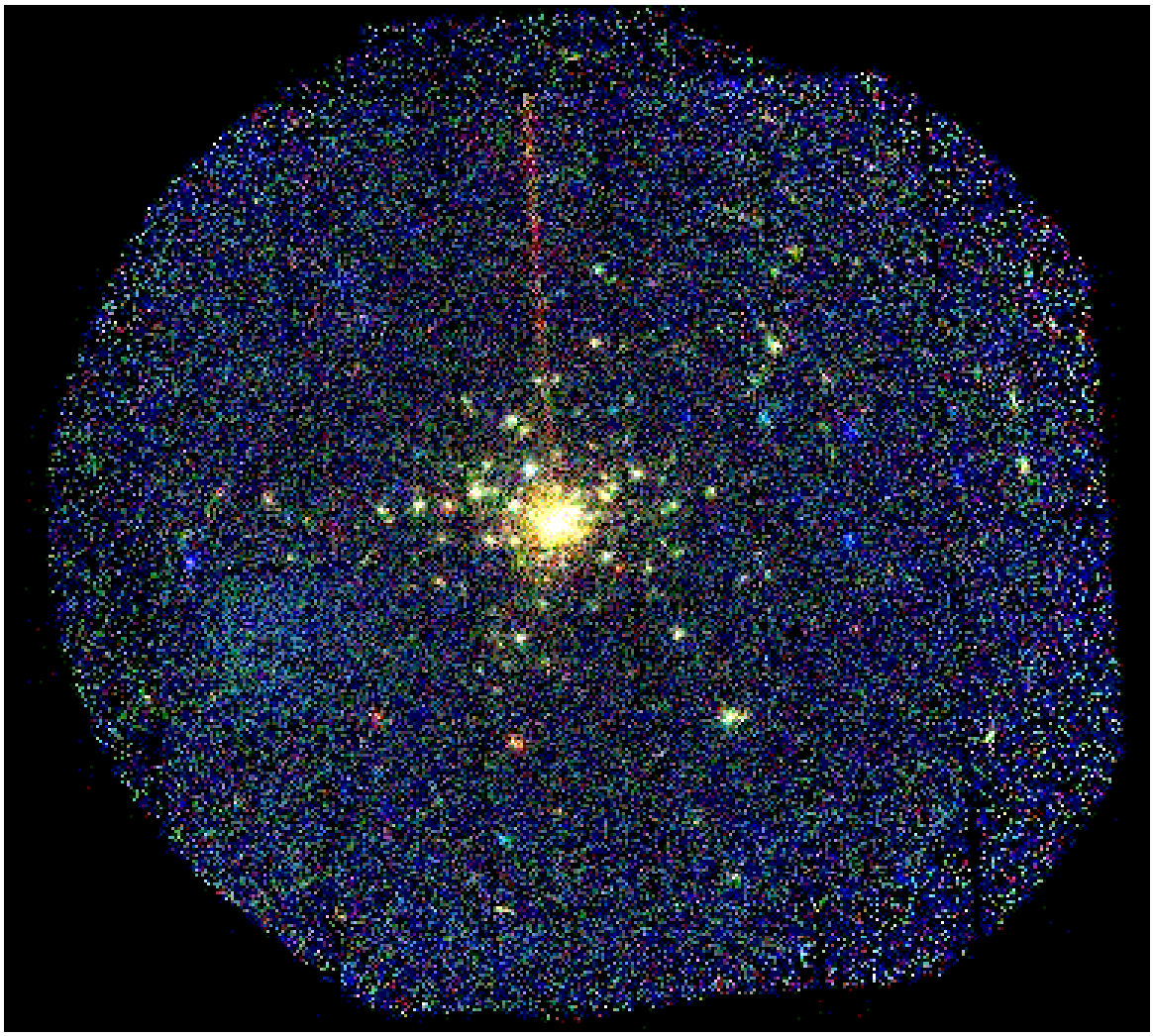

Fig. 1. False colour image of NGC 6383 as derived from the combined EPIC data. The red, green and blue colours correspond to the energy ranges $500 \leq PI \leq 1000$, $1000 < PI \leq 2000$ and $2000 < PI \leq 8000$ respectively. The images in the different energy bands were exposure-corrected before they were combined. North is up, east is left. The radius of the field of view corresponds to about 15 arcmin. The roughly vertical trail above HD 159 176 is produced by events that arrived during the readout of the pn detector (see e.g. Strüder et al. 2001). (This figure is available in color in electronic form.)

and 2.2 respectively. In Sect. 2.3, we investigate the nature of the X-ray sources. Section 3 summarizes our results and presents a discussion of the star formation process in NGC 6383.

2. X-ray sources in the open cluster NGC 6383

NGC 6383 was observed serendipitously with *XMM-Newton* (Jansen et al. 2001) during our AO1 pointing of the massive O-star binary HD 159 176. The observation took place in March 2001 (JD 2 451 977.903 – 2 451 978.338). The two EPIC MOS instruments were operated in the full frame mode (Turner et al. 2001) whilst the EPIC-pn camera was used in the extended full frame mode (Strüder et al. 2001). All three EPIC instruments used the thick filter to reject optical light. We used version 5.2 of the *XMM-Newton* Science Analysis System (SAS) software to process the raw data. Unfortunately, the observation was significantly affected by a high background episode, most probably due to a soft proton flare. While this does not impact on the analysis of the bright central source HD 159 176 (see the discussion by De Becker et al. 2003), it could nevertheless affect the detection and analysis of much fainter sources. Therefore, we filtered out time intervals with a high background level and the remaining useful exposure times were about 15.1, 16.1 and 13.8 ksec for the MOS1, MOS2 and pn detectors respectively. For further details on the observations and the pipeline processing, we refer to the work of De Becker et al. (2003).

The combined EPIC X-ray image around HD 159 176 reveals a number of faint discrete sources displaying a strong concentration towards the O-star binary. Figure 1 shows a false colour image of NGC 6383 where the red, green and blue colours correspond respectively to photons in the pulse invariant (PI) energy channel bands $500 \leq PI \leq 1000$, $1000 < PI \leq 2000$ and $2000 < PI \leq 8000$ (approximately corresponding to energies of [0.5−1.0],]1.0−2.0] and]2.0−8.0] keV)[1]. Most

[1] Hereafter we refer respectively to the soft, medium and hard energy bands.

sources have their spectral distribution peaking between 1.0 and 2.0 keV. Two sources have softer spectra whilst about six sources have significantly harder spectra.

We used the SAS source detection algorithms (see e.g. Hasinger et al. 2001) to derive a list of X-ray sources. We then inspected each source manually to reject false detections due to instrumental artifacts. In this way, we found 77 sources that were detected simultaneously in the MOS1, MOS2 and pn images with a combined logarithmic likelihood given by

$$\mathcal{L} = \sum_{i=1}^{9} -\ln p_i$$

where the summation runs over the three energy band images for each of the MOS1, MOS2 and pn detectors. Here, p_i stands for the probability that a random Poissonian fluctuation of the background may have produced the observed source counts in the image i. This combined logarithmic likelihood $\mathcal{L}$ is then renormalized to a logarithmic likelihood for a single experiment and is finally constrained to be ≥20.0. With this probability threshold, we expect less than one spurious detection due to background fluctuations over the entire EPIC field of view.

The faintest sources in this category have about 2×10^{-3} cts s^{-1} over the entire energy range of the pn camera. Assuming a 1 keV thermal spectrum with a neutral hydrogen column density of $N_{\rm H}^{\rm ISM} = 5.8 \times 10^{21}\,E(B-V) = 1.91 \times 10^{21}$ cm^{-2} (Bohlin et al. 1978), the faintest sources correspond to an observed flux of about 3.6×10^{-15} erg cm^{-2} s^{-1} and an unabsorbed flux of 5.6×10^{-15} erg cm^{-2} s^{-1} in the 0.5–10.0 keV energy range.

The 77 sources are listed in Table 1. The source designation in this table follows the naming conventions recommended by the *XMM* SOC and the IAU: the XMMU J prefix is followed by the right ascension HHMMSS.s (in hours, minutes, seconds and tenths of seconds, equinox J2000) and the declination of the source +/−DDMMSS (in degrees, arcminutes and arcseconds, equinox J2000), both truncated not rounded.

2.1. X-ray properties

For those sources that have a pn count rate of at least 5×10^{-3} cts s^{-1}, Table 1 lists two hardness ratios defined as

$$HR_1 = (M - S)/(M + S)$$

and

$$HR_2 = (H - M)/(H + M)$$

where S, M and H stand respectively for the EPIC-pn count rates in the soft, medium and hard energy bands defined hereabove. Only a few sources (#4, 5 and 6) display hard spectra as indicated also by their blue colours in Fig. 1. To these we can add sources #8 and 18 that display blue colours in Fig. 1, but have no hardness ratio either because they fall close to a gap in the pn detector (#8) or because their pn count rate is below the limit set hereabove (#18). From the analysis of the infrared counterparts of two of these five sources (see below), it appears that these hard spectra are essentially the result of the absorption by large column densities.

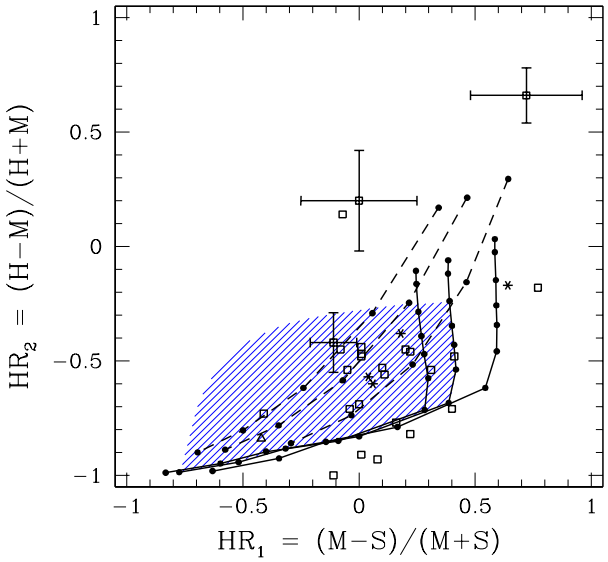

Fig. 2. Hardness ratios HR_1 and HR_2 for the X-ray sources in the field of NGC 6383 (open squares). The open triangle corresponds to HD 159 176, while the asterisks yield four sources for which we studied the spectra (see text). The filled dots exhibit the results for the model simulations described in the text; the lower temperature (or the larger photon indices) correspond to the softer spectra (i.e. the more negative values of HR_1 and HR_2). The solid lines correspond to the simulated thermal plasma models whereas the dashed curves yield the results for power law spectra. For each set of models, the larger hydrogen column density ($2 \times N_{\rm H}$) corresponds to the rightmost curve. For clarity error bars have only been indicated for three sources (#6, 14 and 25). Finally, the shaded area yields the region where objects with $kT_1 \in [0.25{-}1.0]$ keV and $kT_2 \in [1.0{-}4.0]$ (as found for confirmed T Tauri stars) should be found if they suffer an absorption by $N_{\rm H}^{\rm ISM} = 1.91 \times 10^{21}$ cm^{-2} (see text).

The hardness ratios that have an accuracy better than 0.3 are plotted in Fig. 2. In an attempt to relate these hardness ratios to the spectral properties of the sources, we have simulated the values of HR_1 and HR_2 for a grid of simple models. Within XSPEC, we have used the EPIC-pn response matrices to generate fake spectra corresponding either to optically thin thermal plasma MEKAL models (Mewe et al. 1985; Kaastra 1992) or power law energy distributions. For the thermal models, we considered plasma temperatures of kT = 0.25, 0.50, 0.75, 1.0, 1.5, 2.0, 2.5, 3.0, 4.0, 6.0 and 8.0 keV, whilst we simulated power law spectra with photon indices of 1.0, 2.0, 3.0, 4.0 and 5.0. Both types of models were combined with neutral hydrogen column densities of $N_{\rm H}^{\rm ISM} = 1.91 \times 10^{21}$ cm^{-2}, $0.5 \times N_{\rm H}^{\rm ISM}$ and $2 \times N_{\rm H}^{\rm ISM}$. These fake spectra were used to generate the hardness ratio curves displayed in Fig. 2.

Although the error bars on most of the observed hardness ratios are quite large, it can be seen from Fig. 2 that many sources have hardness ratios that are apparently roughly consistent with simple one-component models. However, this does not imply that such models actually fit the spectra of these objects. In fact, the spatial distribution of our sources, as well as the properties of their counterparts (see below), suggest that many of them may belong to the low-mass stellar population of NGC 6383. It is nowadays well known that the

Table 2. Spectral and variability analyses of the brightest X-ray sources in the field of NGC 6383. The neutral hydrogen column density was frozen in the spectral fits at the interstellar value (1.91×10^{21} cm^{-2}). Columns 2 and 3 list the resulting best fit temperatures of the MEKAL components, whilst column 4 provides the reduced χ^2 along with the number of degrees of freedom. Columns 5 and 6 yield the observed and absorption corrected fluxes respectively. The quoted uncertainties correspond to formal errors on the spectral fits.

#	kT_1 (keV)	kT_2 (keV)	χ^2_ν (d.o.f.)	$f_{\rm X,obs}$ (10^{-13} erg cm^{-2} s^{-1})	$f_{\rm X,unabs}$ (10^{-13} erg cm^{-2} s^{-1})	Variability
16	$0.87^{+0.23}_{-0.14}$	$3.17^{+1.68}_{-0.97}$	1.08 (55)	0.81	1.08	No
50	$0.61^{+0.24}_{-0.25}$	$5.52^{+1.98}_{-1.31}$	1.02 (84)	1.27	1.53	Yes
55	$0.33^{+0.34}_{-0.05}$	$2.16^{+0.72}_{-0.43}$	1.18 (73)	0.70	1.06	No
65	$0.73^{+0.13}_{-0.12}$	$2.22^{+0.50}_{-0.38}$	1.04 (71)	0.72	1.02	No

coronal X-ray emission of active late-type stars is generally not monothermal. For instance, Tsujimoto et al. (2002) and Favata et al. (2003) find that the *Chandra* and *XMM-Newton* spectra of confirmed T Tauri stars in the Orion Molecular Cloud and in the L 1551 star formation complex are best represented by 2-T thermal models with kT_1 and kT_2 in the ranges ∼0.25−1.0 keV and ∼1.0–4.0 keV respectively. In this context, one should note that the actual energy distribution of a 2-T thermal plasma might mimic the hardness ratios of a pure power law model. Indeed, for a 2-T thermal plasma, the observed hardness ratio should be a linear combination of the hardness ratios corresponding to the individual temperature components:

$$HR_i = \alpha_i\, HR_i(kT_1) + (1-\alpha_i)\, HR_i(kT_2)$$

where α_i is the ratio between the count rate of the kT_1 component and the total rate over the two energy bands used in the definition of HR_i. The shaded area in Fig. 2 illustrates the region of the HR_1–HR_2 diagram where objects with $kT_1 \in [0.25{-}1.0]$ keV and $kT_2 \in [1.0{-}4.0]$ keV (as found for confirmed T Tauri stars, see above) should be found if they suffer an absorption by a column density $N_{\rm H}^{\rm ISM} = 1.91 \times 10^{21}$ cm^{-2}. We see that most of our NGC 6383 EPIC sources lie inside the shaded area. While this is by no means a proof that these objects have indeed 2-T thermal spectra, it shows that at least their properties are not inconsistent with such a model.

The properties of HD 159 176 (source #44) have been discussed by De Becker et al. (2003) and we will not repeat this analysis here. Let us simply recall that the EPIC and RGS spectra could neither be fitted with a 1-T thermal model nor a pure power law energy distribution. A 2-T MEKAL model yielded a better fit with $N_{\rm H} \sim 0.53 \times 10^{22}$ cm^{-2}, $kT_1 \sim 0.20$ and $kT_2 \geq 0.60$ keV. The location of HD 159 176 in Fig. 2 reflects the rather soft spectrum of this source. It should be noted that although the position of HD 159 176 in the $HR_1 - HR_2$ plane falls close to the locus of pure power law models, such a model is clearly at odds with the RGS and EPIC spectra of this star (De Becker et al. 2003).

In addition to HD 159 176, four sources (#16, 50, 55 and 65) have sufficiently large count rates for a more detailed study of their spectra and light curves. Background corrected spectra were rebinned to have at least 9 counts per energy channel and the three EPIC spectra were analysed simultaneously using the XSPEC software. We attempted to fit the spectra with 1-T thermal plasma MEKAL models. The reduced χ^2 values are quite large. Better fits are obtained if we consider 2-T MEKAL models. Table 2 lists the results of the 2-T fits with the neutral hydrogen column density frozen at the mean interstellar value (1.91×10^{21} cm^{-2} see above). Alternatively, we have also allowed the hydrogen column density to float as a free parameter. The best fit parameters are always very close to those listed in Table 2, except for source #55. For this source, a slightly better fit is achieved with a neutral hydrogen column density $\leq 0.06 \times 10^{22}$ cm^{-2} and the corresponding best fit temperatures are 0.83 and 3.15 keV. This result suggests that source #55 might be a foreground object (see also below) affected by a lower column density than the actual cluster members. The four sources have X-ray spectra that consist of a component with a temperature between 0.5 and 1.0 keV and a second much hotter component with kT_2 of order 2−5 keV. The hottest component is observed for source #50, i.e. the source that undergoes a flare during our observation (see below). The average EPIC-pn count rate to unreddened flux conversion factor for the three sources #16, 50 and 65 amounts to 5.1×10^{-12} erg cm^{-2} count^{-1}. Assuming that this conversion factor applies to all the sources in the field of view, our lower detection count rate of 2×10^{-3} cts s^{-1} corresponds to a limiting sensitivity of 10^{-14} erg cm^{-2} s^{-1} on the unabsorbed flux.

X-ray light curves corrected for good time intervals were extracted for the four brighter sources and for all three EPIC cameras. We checked these light curves for variability and for consistency between the various instruments. The only source that displays a strong and well correlated variability in the light curves of all three instruments is #50. This source undergoes a strong X-ray flare towards the end of our observation (see Fig. 3). At the onset of this flare, the X-ray flux rises by about an order of magnitude within about 3000 s. This feature is quite reminiscent of the flare observed on the pre-main sequence star SCB 731 in NGC 6530 (Rauw et al. 2002) and on other PMS objects (see e.g. Feigelson & Montmerle 1999; Preibisch & Zinnecker 2002). We note that the spectrum of the source appears significantly harder during the eruption. In fact, whereas the soft band dominates the count rate during the quiescence, Fig. 3 indicates that the medium and, shortly after, also the hard band overtake the soft band during the flare. This spectral hardening is again quite similar to the behaviour of other flaring PMS stars (e.g. Preibisch & Zinnecker 2002).

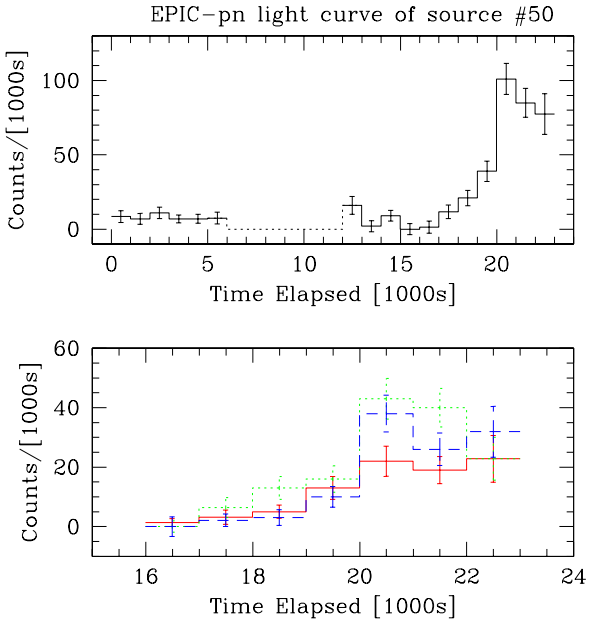

Fig. 3. EPIC-pn light curve of source #50. Upper panel: corrected source count rate as a function of time elapsed since JD 2 451 978.072. The source counts have been binned into intervals of 1000 s corrected for the good time intervals and have been corrected for the background variations. Note that the interval with zero count rate (dotted line) corresponds to a soft proton flare that was discarded from our data set. Lower panel: zoom on the flare as seen in different energy bands. The soft, medium and hard band light curve are displayed by the continuous, dotted and dashed line respectively. Before the flare, the mean count rates were respectively 3.8×10^{-3}, 1.2×10^{-3} and 1.2×10^{-3} cts s^{-1} in the *S*, *M* and *H* energy bands.

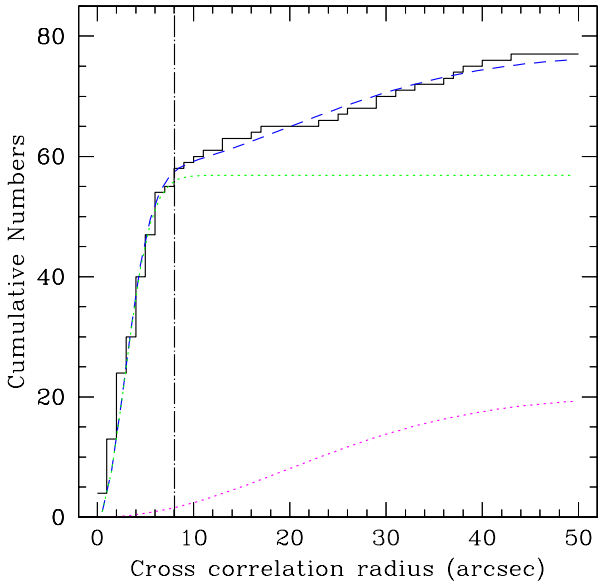

Fig. 4. Cumulative numbers of correlations between the X-ray detections and the USNO catalogue objects as a function of the correlation radius. The dotted curves correspond to the best fitting expressions for the real and spurious correlations. The dashed curve yields the sum of these terms and the dash-dotted vertical line corresponds to the adopted correlation radius of 8 arcsec.

2.2. Optical and infrared counterparts

We have cross-correlated the positions of the 77 sources with various catalogues. Unfortunately, there exists no dedicated very deep photometric survey of NGC 6383 in the literature. Therefore, we used the US Naval Observatory (USNO, Monet et al. 1998), the Guide Star Catalogue (GSC, version 2.2)[2] and the Two Micron All Sky Survey[3] (2MASS, Skrutskie et al. 1997) catalogues. In order to determine the optimal radius of cross-correlation, we adopted the approach outlined by Jeffries et al. (1997) and applied to the *XMM-Newton* data of the very young open cluster NGC 6530 by Rauw et al. (2002): the distribution of the cumulative number of catalogued sources as a function of the cross-correlation radius r (see Fig. 4) is modelled by

$$\Phi(d \le r) = A\left[1 - \exp\left(\frac{-r^2}{2\,\sigma^2}\right)\right] + (N - A)\left[1 - \exp\left(-\pi\,B\,r^2\right)\right]$$

where N, A, σ and B stand respectively for the total number of cross-correlated X-ray sources ($N = 77$), the number of true correlations, the uncertainty on the X-ray source position and the surface density of catalogue sources. The first term in the expression of $\Phi(d \le r)$ stands for the cumulative distribution of true correlations whereas the second term yields the cumulative number of spurious correlations (see Jeffries et al. 1997). A, σ and B are fitting parameters and were obtained from the best fit to the actual distribution displayed in Fig. 4. For the USNO catalogue, we derive $A = 56.9$, $\sigma = 2.8$ arcsec and $B = 4.1 \times 10^{-4}$ arcsec^{-2}. The optimal correlation radius, i.e. the radius that includes the majority of the true correlations while simultaneously limiting contamination by spurious correlations, is found to be around 8 arcsec. For $r = 8$ arcsec, we expect to statistically achieve 56 true and less than 2 spurious correlations. For the 2MASS catalogue, we obtain very similar numbers and therefore we consider an optical or infrared source as a possible counterpart if it falls within 8 arcsec of the coordinates of the X-ray source.

The degradation of the point spread function (PSF) of the *XMM* mirror modules with increasing off-axis angle (Stockman et al. 1998) could bias the value of the optimal correlation radius. For a uniform distribution of sources over the entire field of view, one might have to consider the correlation radius as a function of the off-axis angle. However, in the case of our data set, most of the sources lie within less than 6 arcmin from the center and using a constant correlation radius should therefore provide a fairly good approximation.

The results of the correlations with the USNO and 2MASS catalogues are listed in Table 1:

- 57 EPIC sources have a single USNO or GSC optical counterpart within a radius of less than 8 arcsec. The average angular separation between the X-ray source and the optical

[2] The Guide Star Catalogue-II is a joint project of the Space Telescope Science Institute and the Osservatorio Astronomico di Torino.

[3] We used the 2MASS all-sky point source catalogue released in March 2003 and available at `http://irsa.ipac.caltech.edu/`

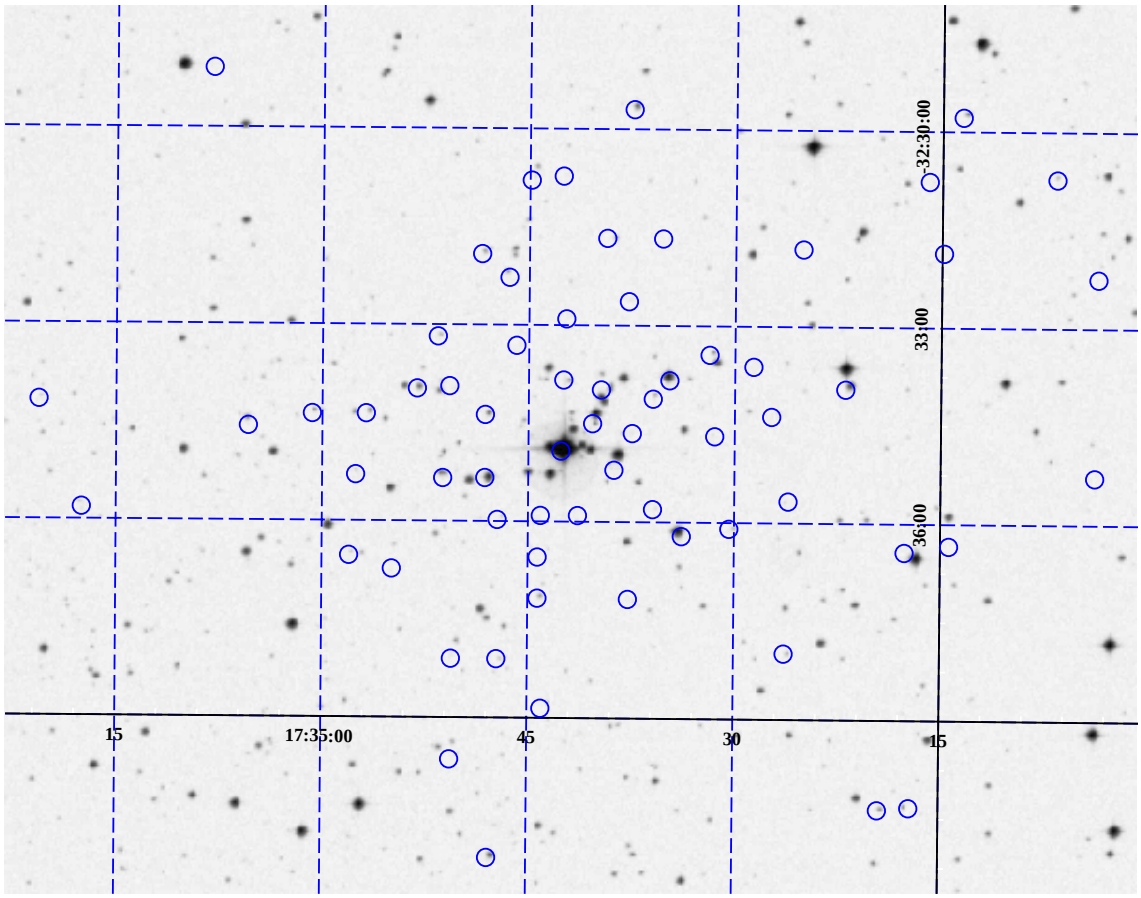

Fig. 5. Location of the X-ray sources detected with *XMM-Newton* around HD 159 176 overlaid on a Digital Sky Survey *V* image. The circles have radii of 8 arcsec corresponding to the optimal cross-correlation radius.

counterpart is (3.6 ± 2.0)″. Most optical counterparts are faint and only a few objects have HD numbers or a number in one of the Thé (Thé 1985), FJL (FitzGerald et al. 1978) or LE (Lloyd Evans 1978) catalogues (see Table 3). Except for the latter objects, the photometric data are taken from the GSC and USNO catalogues and refer hence to photographic magnitudes. All of these 57 sources have at least one 2MASS infrared counterpart, but only 23 X-ray sources have a single USNO and a single 2MASS counterpart[4].

- 29 EPIC sources are found to have a single 2MASS counterpart.
- 11 EPIC sources are found to have two or more USNO or GSC sources in the 8 arcsec radius. The number of EPIC sources having more than one 2MASS counterpart is much larger (47).
- 9 EPIC sources have neither an USNO nor a GSC counterpart, while there is only one source (#5) that has neither an optical nor an infrared counterpart. Note that this object has a very hard X-ray spectrum as revealed by its blue colour in Fig. 1 and its HR_2 value (≥0.91) in Table 1. This source is therefore likely a heavily absorbed background object.

[4] Since the positional errors on the USNO sources are of order 0.3″in both RA and DEC whilst the corresponding errors for the 2MASS catalogue are of order 0.1″, the small positional discrepancies between the optical and IR counterparts are probably not significant.

Table 3. X-ray sources with bright optical counterparts that are known from other catalogues than the USNO or GSC. The last column yields the reference for the spectral type (FJL = FitzGerald et al. 1978, vdA = van den Ancker et al. 2000). The photometric data are taken from FJL, except for Thé 7 and 26 for which we adopt results from Eggen (1961).

#	cross-ID	V	$B-V$	Spect. type	Ref.
17	Thé 7	12.73	0.32		
24	Thé 26	12.87	0.76	A1 IV	vdA
26	HD 317 857	10.30	0.29	B8 IV/B9 IV	FJL, vdA
27	HD 317 847	10.33	0.10	B2 V	FJL
38	FJL 7	12.62	0.28		
39	FJL 9	10.84	0.14		
42	FJL 11	15.10	1.06		
44	HD 159 176	5.64	0.04	O7 V + O7 V	FJL
55	FJL 23	13.79	0.95	G5 V	vdA
56	FJL 24	11.35	0.18	B8 Vne/B7 V	FJL, vdA

2.3. The nature of the X-ray sources

Most of the optically bright sources (except HD 159 176, HD 317 847 and HD 317 857, see Table 3 and Fig. 5) are not detected in our EPIC images. The bulk of the entries in Table 1 are therefore X-ray sources with a large L_X/L_{vis} ratio. Given the position of the cluster very near the direction of the galactic center (l_{II} = 355.69°, b_{II} = +0.04°), the total galactic column

density along the line of sight in this direction must be extremely large. At low energies the total galactic column probably prevents us from detecting background sources, but maybe some of the very hard sources (like #5) might be associated with extragalactic objects.

It is interesting to compare the list of X-ray sources with a single optical counterpart to the list of PMS candidates listed in the literature. First of all, we note that none of the variable sources from Lloyd Evans (1978) is detected with *XMM*. On the other hand, three of the PMS candidates listed by FitzGerald et al. (1978) are clearly seen in our EPIC images. These are FJL 11 (#42), FJL 23 (#55) and FJL 24 (#56). FJL 23 and 24 are known to display near IR excess emission (Thé et al. 1985; van den Ancker et al. 2000) and star FJL 24 was suggested to be an early-type flare star with episodic Balmer emission lines in its spectrum (FitzGerald et al. 1978). The spectral type of FJL 23 (G5 V) as proposed by van den Ancker et al. (2000) suggests that this might be a foreground object unrelated to NGC 6383. This result is in good agreement with our finding that the source #55 associated with this star might have a smaller hydrogen column density than the average value of the cluster. Thé et al. and van den Ancker et al. noted the presence of a strong IR excess associated with FJL 4, 5 and 6 (all classified as A-type stars) making these three stars other PMS candidates. We note that none of the latter three objects is detected in our data.

Figure 6 illustrates the JHK_s colour–colour diagram of the 2MASS infrared counterparts. The diagram includes only those objects that were detected in all three filters J (1.25 μm), H (1.65 μm) and K_s (2.17μm) with a decent photometric accuracy ($\sigma \leq 0.10$). The intrinsic colours of dwarfs and giants (taken from Bessell & Brett 1988) are indicated by the solid lines, whereas the two upper dashed lines delimit the reddening band for normal dwarf stellar atmospheres adopting the reddening law quoted by Rieke & Lebofsky (1985). While most 2MASS counterparts cluster near the loci of unreddened main sequence and giant stars, sixteen IR sources correspond clearly to heavily reddened objects with A_V up to ~28 mag in the most extreme cases.

Lada & Adams (1992) have shown that the location of a pre-main sequence object in the infrared colour–colour diagram is determined to a large extent by its evolutionary state. Deeply embedded class I protostars were found to lie in the region of the *J–H* vs. H–K_s plane characterized by a large extinction and for the most part to the right of the reddening band. On the other hand, classical and weak-line T Tauri stars suffer a much lower circumstellar extinction. The weak-line T Tauri stars (wTTs) lie within the reddening band of main sequence stars, whereas the classical T Tauri stars (cTTs) have infrared excesses produced by circumstellar disks and fall therefore mostly to the right of the reddening band. Meyer et al. (1997) emphasized that the locus of dereddened JHK colours of PMS stars with circumstellar material is surprisingly narrow and can be described by a simple linear relation between $J-H$ and $H-K$. This relation is shown in Fig. 6 by the dotted straight line[5].

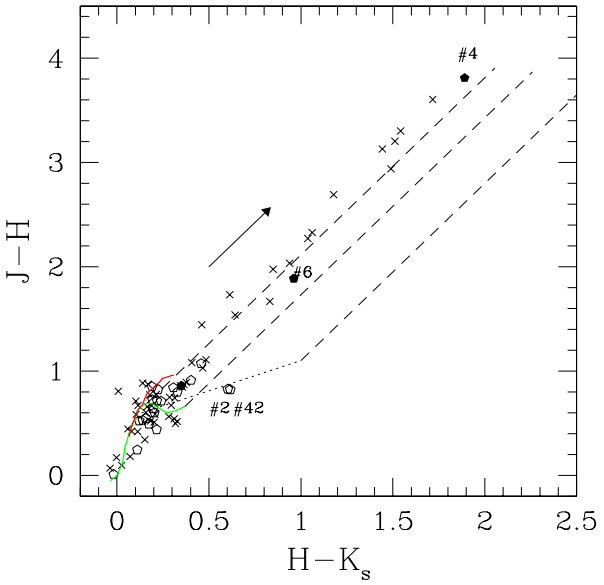

Fig. 6. JHK_s colour–colour diagram of the IR counterparts falling within the 8 arcsec correlation radius from an X-ray source. The heavy solid lines yield the intrinsic colours of main sequence and giant stars, whereas the reddening band is illustrated for up to 30 mag of visual extinction from the position where it intersects the locus of unreddened main sequence stars. Single counterparts of X-ray sources are displayed by pentagons. Open pentagons stand for stars that have also an USNO or GSC counterpart, whilst filled symbols correspond to IR stars without optical counterpart. The crosses indicate IR objects associated with X-ray sources having multiple 2MASS counterparts. The dotted straight line yields the locus of dereddened colours of classical T Tauri stars according to Meyer et al. (1997). See the text for further details.

Inspection of Fig. 6 suggests that only two sources (#2 and 42) fall near the locus of stars with IR excesses revealing the presence of circumstellar material. One of them (#42) is FJL 11 that was already classified as a PMS candidate by FitzGerald et al. (1978). On the other hand, sixteen IR sources suffer a large optical extinction and could therefore be candidates for deeply embedded class I objects. The most extreme reddening ($A_V \simeq 28$ mag) is found for source #4 that has no optical counterpart and displays a very hard X-ray emission. Source #6, another hard X-ray source, suffers a less extreme, but still quite substantial, extinction ($A_V \simeq 11$ mag). The other fourteen objects with $A_V > 5$ mag are not unique counterparts and most importantly the X-ray sources were not found to display extremely hard spectra. Therefore, some of these latter IR objects might actually be unrelated to the X-ray sources.

In summary, our analysis of the 2MASS counterparts indicates that at least two X-ray sources (#2 and 42) are probable PMS objects surrounded by circumstellar material whilst at least two other objects (#4 and 6) are either candidates for deeply embedded class I protostars or are heavily absorbed background objects perhaps unrelated to NGC 6383.

[5] Note however that Preibisch & Zinnecker (2002 and references therein) showed that for the young open cluster IC 348 there exists no strict one-to-one relation between PMS stars with IR excesses and cTTs detected through their strong Hα emission: while all known cTTs in IC 348 are found to have IR excesses, many wTTs also display IR excess emission.

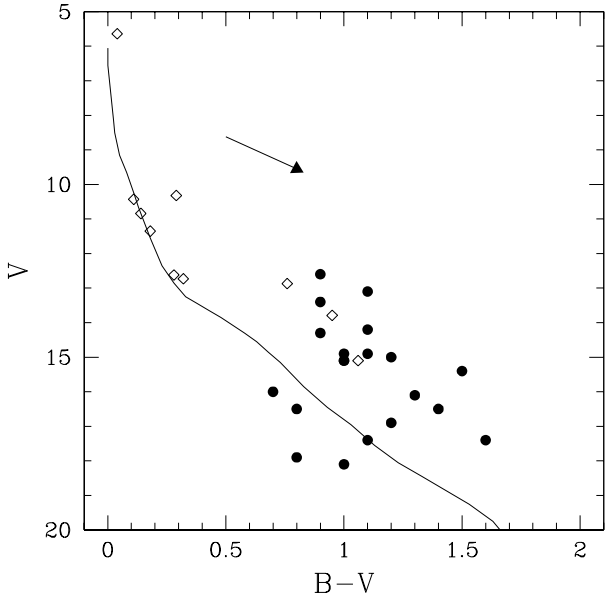

Fig. 7. Colour–magnitude diagram of the X-ray sources with a single optical counterpart and with an existing $B-V$ colour in the very young open cluster NGC 6383. Filled dots indicate stars with USNO/GSC photometry, while the photometric data for the open diamonds are taken from Table 3. The reddening vector with $R_V = 3.1$ is indicated and the solid line shows the ZAMS relation taken from Schmidt-Kaler (1982) shifted by a distance modulus $DM = 10.73$ and reddened with $E(B-V) = 0.33$.

We have plotted those objects for which we have V magnitudes and $B-V$ colours in a colour–magnitude diagram (see Fig. 7). While the optical counterparts brighter than $V \sim 13$ fall mainly on the NGC 6383 main sequence, it appears that most of the sources that are optically fainter lie above the zero age main sequence. Although it is likely that our sample is affected by a number of field interlopers, the strong concentration of faint X-ray sources towards the cluster core together with their optical photometry suggest that many of the EPIC sources with faint optical counterparts are indeed associated with low- and intermediate-mass pre-main sequence stars.

Using the $T_{\rm eff}$ versus $(B-V)_0$ calibration and the bolometric corrections for main-sequence stars from Kenyon & Hartmann (1995), we can construct the Hertzsprung-Russell diagram of the X-ray sources with a single optical counterpart. Comparing this diagram with the pre-main sequence evolutionary tracks of Siess et al. (2000) for $Z = 0.02$, we could in principle infer the masses and ages of the PMS stars. The available USNO and GSC photometry suggests that the bulk of those stars having a location consistent with a PMS status would appear to have masses between 1.0 and 3.0 $M_\odot$ and ages ranging from ∼1.5 to 10 Myr. However, we caution that more accurate optical photometry is needed to firmly establish the properties of these objects. For instance, many X-ray sources with a single optical counterpart are too weak in B to have $B-V$ colours in the USNO or GSC catalogues and they are therefore not considered here. Deeper optical photometry, including also a search for faint Hα emission, is thus needed for a more complete investigation of the nature of the X-ray sources and of the PMS content of NGC 6383.

It is worth noting that out of the twelve B-type stars listed by Thé (1965) and van den Ancker et al. (2000) only three are detected. These are HD 317 857 (B9 IV), HD 317 847 (B2 V) and FJL 24 (B8 V ne). The bulk of the other B-stars in NGC 6383 classified in the literature are later than B5. HD 317 857 is believed to be a foreground object (Thé et al. 1985). FitzGerald et al. (1978) further noted that HD 317 857 has a faint close (∼2 arcsec separation) companion. Whether the X-ray emission comes from the late B-star or from its faint companion is impossible to tell with the present data.

3. Discussion and conclusions

From the previous section, it turns out that an important fraction of the X-ray sources in NGC 6383 might be candidates for PMS objects. Evidence for this interpretation comes from

- The concentration of X-ray sources towards the cluster center indicating that the X-ray sources are actually associated with the cluster.
- The flaring behaviour of source #50: T Tauri PMS stars are usually variable X-ray emitters that exhibit flares with a fast rising light curve followed by a slower decay (Feigelson & Montmerle 1999).
- The spectral properties of the X-ray brightest sources: indeed, T Tauri PMS stars display multi-temperature thermal X-ray spectra with (on average) a soft component in the range $kT_1 \in [0.25-1.0]$ keV and a harder component with $kT_2 \in [1.0-4.0]$ keV (Feigelson & Montmerle 1999; Tsujimoto et al. 2002; Favata et al. 2003).
- The X-ray luminosities: assuming a distance of 1.4 kpc and an EPIC-pn count rate to unreddened flux conversion factor of 5.1×10^{-12} erg cm^{-2} count^{-1}, we find that the faintest sources should have luminosities of 2.4×10^{30} erg s^{-1} (if we adopted the $kT = 1$ keV model instead, the luminosity would be half this value), whilst the flaring source #50 reaches 3.6×10^{31} erg s^{-1}. Indeed, PMS stars are known to have X-ray luminosities of order 10^{30} erg s^{-1}, i.e. about 10^3 times larger than that of the Sun (Neuhäuser 1997). For the sources with a single counterpart, $\log(L_{\rm X}/L_{\rm bol})$ increases from about −5.5 for the late B stars to ∼−3 for the low-mass stars, a value quite typical for X-ray bright PMS stars (see Fig. 8)[6].

FitzGerald et al. (1978) suggested that the star formation process in the core of NGC 6383 might be triggered by the massive binary HD 159 176. These authors derived an age of 1.7 ± 0.4 Myr for the stars in the ∼1.25 arcmin radius cluster core, whereas they estimated that HD 159 176 is 2.8 ± 0.5 Myr old. The concentration of faint X-ray sources around HD 159 176 suggests indeed that there must be a connection between the PMS objects and the massive binary. However, the way massive

[6] The apparent trend of $\log(L_{\rm X}/L_{\rm bol})$ with M_V seen in Fig. 8 should not be over interpreted. In fact the X-ray production in the objects at the higher luminosity end (shocks in the winds of B-type stars or unseen low-mass companions?) and those at the fainter end (coronal sources and late-type PMS-like emission) arises most probably through quite distinct physical mechanisms.

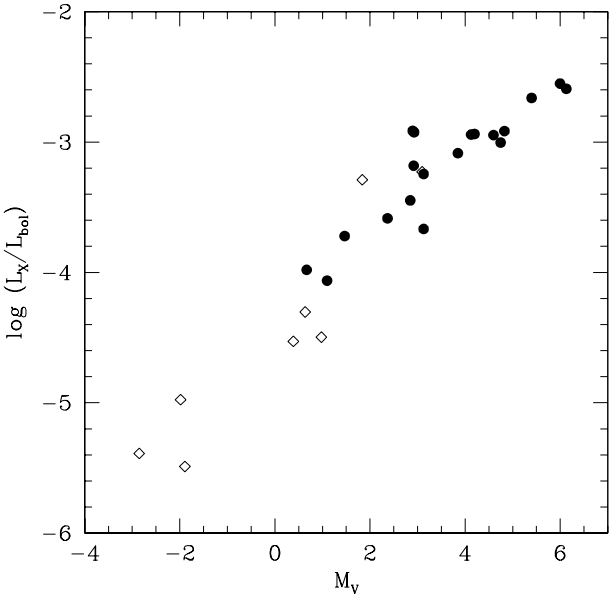

Fig. 8. Ratio between the X-ray luminosity and the bolometric luminosity of the EPIC sources with a single optical counterpart as a function of the absolute magnitude M_V (assuming the stars belong to NGC 6383). The symbols have the same meaning as in Fig. 7. Note that we have omitted sources #27 (no reliable X-ray count rate) and #44 (HD 159 176, discussed by De Becker et al. 2003).

stars form is still a controversial question and another scenario might equally well account for the possible connection between HD 159 176 and the PMS stars in NGC 6383. Bonnell & Bate (2002) performed *N*-body simulations of an open cluster containing 1000 protostars and a large amount of gas. They found that gas accretion leads to a strong contraction of the cluster and hence the stellar density in the simulated cluster core becomes sufficient for a significant number of stellar collisions to occur. In this scenario, the most massive stars of the cluster are formed through a combination of gas accretion and stellar mergers. The massive objects formed this way in the simulations are generally members of binary systems. NGC 6383 might fit rather well into this scenario: HD 159 176, the most massive object of the cluster is a binary system sitting in the core and the concentration of low-mass young stellar objects as revealed by their X-ray emission is much larger in the core than in the outer regions of the cluster. A crucial issue to address in future studies of this cluster will therefore be an accurate determination of the ages of its various components.

Finally, let us emphasize that, so far, there is evidence for only a few PMS stars with circumstellar material among the PMS candidates detected in our EPIC data. In fact, 2MASS colours of their infrared counterparts reveal the infrared excesses that would be expected for such objects only in two cases. It should be stressed that the modest number of 2MASS counterparts displaying a clear IR excess related to circumstellar material does not rule out that the X-ray sources might be associated with magnetically active PMS stars. Indeed, in the Chamaeleon I cloud, Feigelson et al. (1993) found that most X-ray selected PMS stars were wTTs without prominent circumstellar material. Similar results were obtained for the Orion Molecular Cloud (Tsujimoto et al. 2002).

Also there is little known about Hα emission among the cluster members of NGC 6383. At first sight, this observation suggests that most of our PMS candidates may be weak-line T Tauri stars and that they may be intrinsically X-ray brighter than classical T Tauri stars. Similar conclusions were reached for the T Tauri stars in the Taurus-Auriga-Perseus complex (Stelzer & Neuhäuser 2001) and NGC 6530 (Rauw et al. 2002). However, Preibisch & Zinnecker (2001, 2002) pointed out that *Chandra* observations of IC 348 provide no evidence for a significant difference in the X-ray properties of both classes of T Tauri stars and the apparent difference in the luminosities of the Taurus-Auriga-Perseus and NGC 6530 objects might in fact be a pure selection effect. Deep Hα photometry is therefore urgently needed to identify classical and weak-line T Tauri stars in NGC 6383.

Acknowledgements. Our thanks go to Mathias Ehle (*XMM*-SOC) for his help in processing the EPIC data, to Alain Detal (Liège) for his help in installing the SAS and to the referee, Dr. M. van den Ancker, whose comments helped to significantly improve our manuscript. The Liège team acknowledges support from the Fonds National de la Recherche Scientifique (Belgium) and through the PRODEX XMM-OM and Integral Projects. This research is also supported in part by contracts P4/05 and P5/36 "Pôle d'Attraction Interuniversitaire" (SSTC-Belgium). JMP gratefully acknowledges funding from PPARC for a PDRA position. This research has made use of the SIMBAD database, operated at CDS, Strasbourg, France and NASA's Astrophysics Data System Abstract Service. This publication makes also use of data products from the Two Micron All Sky Survey, which is a joint project of the University of Massachusetts and the Infrared Processing and Analysis Center, funded by NASA and the NSF.

References

Bessell, M. S., & Brett, J. M. 1988, PASP, 100, 1134
Bohlin, R. C., Savage, B. D., & Drake, J. F. 1978, ApJ, 224, 132
Bonnell, I. A., & Bate, M. R. 2002, MNRAS, 336, 659
De Becker, M., Rauw, G., Pittard, J. M., et al. 2003, A&A, submitted
Eggen, O. J. 1961, Roy. Greenwich Obs. Bull., 27, 61
Favata, F., Giardino, G., Micela, G., Sciortino, S., & Damiani, F. 2003, A&A, 403, 187
Feigelson, E. D., Casanova, S., Montmerle, T., & Guibert, J. 1993, ApJ, 416, 623
Feigelson, E. D., & Montmerle, T. 1999, ARA&A, 37, 363
FitzGerald, M. P., Jackson, P. D., Luiken, M., Grayzeck, E. J., & Moffat, A. F. J. 1978, MNRAS, 182, 607
Hasinger, G., Altieri, B., Arnaud, M., et al. 2001, A&A, 365, L45
Jansen, F., Lumb, D., Altieri, B., et al. 2001, A&A, 365, L1
Jeffries, R. D., Thurston, M. R., & Pye, J. P. 1997, MNRAS, 287, 350
Kaastra, J. S. 1992, An X-ray spectral code for optically thin plasmas, Internal SRON-Leiden Report
Kenyon, S. J., & Hartmann, L. 1995, ApJS, 101, 117
Lada, C. J., & Adams, F. C. 1992, ApJ, 393, 278
Lloyd Evans, T. 1978, MNRAS, 184, 661
Mewe, R., Gronenschild, E. H. B. M., & van den Oord, G. H. J. 1985, A&AS, 62, 197
Meyer, M. R., Calvet, N., & Hillenbrand, L. A. 1997, AJ, 114, 288

Monet, D., Bird, A., Canzian, B., et al. 1998, USNO V2.0, A catalogue of Astrometric Standards, U.S. Naval Observatory Flagstaff Station (USNOFS) and Universities Space Research Association (USRA) stationed at USNOFS
Neuhäuser, R. 1997, Science, 276, 1363
Preibisch, T., & Zinnecker, H. 2001, AJ, 122, 866
Preibisch, T., & Zinnecker, H. 2002, AJ, 123, 1613
Rauw, G., Nazé, Y., Gosset, E., et al. 2002, A&A, 395, 499
Rieke, G. H., & Lebofsky, M. J. 1985, ApJ, 288, 618
Schmidt-Kaler, T. 1982, in Physical Parameters of the Stars, Landolt-Börnstein Numerical Data and Functional Relationships in Science and Technology, Group VI, vol. 2b
Sharpless, S. 1953, ApJ, 118, 362
Siess, L., Dufour, E., & Forestini, M. 2000, A&A, 358, 593
Skrutskie, M. F., Schneider, S. E., Stiening, R., et al. 1997, in The Impact of Large Scale Near-IR Sky Surveys, ed. F. Garzon et al. (Dordrecht: Kluwer Acad. Pub.), 25
Stelzer, B., & Neuhäuser, R. 2001, A&A, 377, 538
Stockman, Y., Barzin, P., Hansen, H., et al. 1998, in Proc. First XMM Workshop on Science with XMM, ed. M. Dahlem, (`http://xmm.vilspa.esa.es/external/xmm_science/1st_workshop`)
Strüder, L., Briel, U., Dennerl, K., et al. 2001, A&A, 365, L18
Sugizaki, M., Mitsuda, K., Kaneda, H., et al. 2001, ApJS, 134, 77
Sung, H., Chun, M.-Y., & Bessell, M. S. 2000, AJ, 120, 333
Thé, P. S. 1965, Contr. Bosscha Obs., Lembang, 32
Thé, P. S., Hageman, T., Westerlund, B. E., & Tijn A Djie, H. R. E. 1985, A&A, 151, 391
Tsujimoto, M., Koyama, K., Tsuboi, Y., Goto, M., & Kobayashi, N. 2002, ApJ, 566, 974
Turner, M. J. L., Abbey, A., Arnaud, M., et al. 2001, A&A, 365, L27
van den Ancker, M. E., Thé, P. S., & de Winter, D. 2000, A&A, 362, 580

Online Material

Table 1. X-ray sources detected in our EPIC images of NGC 6383. The first and second columns yield the number of the X-ray source as well as the name according to the naming conventions for serendipitous *XMM-Newton* sources. Columns 3, 4 and 5 provide the vignetting and background corrected EPIC-pn and MOS count rates in the 0.5–10.0 keV energy range, whilst Cols. 6 and 7 yield the HR_1 and HR_2 hardness ratios evaluated from the pn data (see the definition of HR_1 and HR_2 in the text). Columns 8 to 12 and 13 to 17 summarize the results of the cross-correlation with the USNO (and GSC) and 2MASS catalogues respectively. Columns 8 and 13 yield the numbers of optical and IR counterparts within 8 arcsec from the X-ray source, while Cols. 9 and 14 provide the angular separation for single counterparts.

#	XMMU J	pn	MOS1	MOS2	HR_1	HR_2	USNO (and GSC)					2MASS				
							Nr.	d	B	V	R	Nr.	d	J	H	K_S
		10^{-3} cts s^{-1}	10^{-3} cts s^{-1}	10^{-3} cts s^{-1}				($''$)					($''$)			
[1]	[2]	[3]	[4]	[5]	[6]	[7]	[8]	[9]	[10]	[11]	[12]	[13]	[14]	[15]	[16]	[17]
1	173 340.4−323 310	18.6 ± 3.1	7.9 ± 2.5	12.0 ± 2.7	−0.05 ± 0.17	−0.54 ± 0.28	1	1.7	15.9	14.9	14.3	4				
2	173 341.6−323 121	7.4 ± 2.6	2.5 ± 1.8	7.3 ± 2.5	0.19 ± 0.26	−0.42 ± 0.41	1	3.3	16.1	15.1	14.5	1	3.2	12.7	11.9	11.3
3	173 344.8−324 052	11.4 ± 3.0	9.4 ± 2.8		0.41 ± 0.22	−0.48 ± 0.28	1	0.6	14.3	13.4	13.0	2				
4	173 349.0−323 332	6.4 ± 1.6	0.9 ± 1.2	2.9 ± 1.5	0.58 ± 0.42	0.69 ± 0.17	0					1	3.6	15.9	12.0	10.1
5	173 403.5−323 214	6.4 ± 1.5	3.8 ± 1.4	4.2 ± 1.3		≥0.91	0					0				
6	173 403.7−323 516	10.2 ± 1.6	4.6 ± 1.3	4.5 ± 1.2	0.72 ± 0.24	0.66 ± 0.12	0					1	2.1	13.3	11.5	10.5
7	173 406.6−323 043	5.5 ± 1.5	2.9 ± 1.2	2.8 ± 1.1	−0.37 ± 0.35	0.39 ± 0.36	1	2.2	17.4	16.1	15.5	4				
8	173 413.4−322 946		9.0 ± 1.7	16.9 ± 2.0			1	3.6	15.3	14.2	13.9	1	3.4	12.2	11.7	11.6
9	173 414.2−322 317	7.3 ± 1.9	3.2 ± 1.6	1.8 ± 1.7	−0.33 ± 0.33	0.41 ± 0.31	2					2				
10	173 414.3−323 620	3.8 ± 1.1	1.0 ± 0.6	1.8 ± 0.7			0					2				
11	173 414.8−323 151	8.1 ± 1.5	4.1 ± 1.0	3.0 ± 0.9	0.77 ± 0.19	−0.18 ± 0.21	1	3.5			17.9	1	3.4	13.5	12.4	12.0
12	173 415.9−323 046	3.3 ± 1.1	1.6 ± 0.8	1.6 ± 0.7			1	2.3	19.0	17.4	16.6	1	2.3	(14.4)	13.2	12.9
13	173 417.1−324 020	2.8 ± 1.4	1.8 ± 1.1	2.6 ± 1.1			1	6.8	16.1	15.1	14.6	2				
14	173 417.5−323 626	6.1 ± 1.1	2.6 ± 0.9	1.8 ± 0.7	−0.00 ± 0.25	0.20 ± 0.22	0					1	1.6	15.2	14.4	(14.0)
15	173 418.8−324 455	5.9 ± 2.0	3.5 ± 1.6	3.6 ± 1.3	−0.09 ± 0.37	≤0.35	1	2.2			17.6	1	2.1	14.2	13.4	13.1
16	173 419.3−324 022	19.6 ± 2.3	15.6 ± 2.1	13.7 ± 1.8	0.18 ± 0.12	−0.38 ± 0.15	1	1.8	16.0	14.9	14.2	1	1.6	12.5	12.0	11.8
17	173 421.9−323 357	6.4 ± 1.1	4.4 ± 1.0	3.5 ± 0.9	0.08 ± 0.16	≤−0.67	1	3.8		12.3	12.4	1	3.5	11.6	11.4	11.2
18	173 425.0−323 149	2.2 ± 1.0	2.2 ± 0.8	1.9 ± 0.7			0					3				
19	173 426.0−323 540	4.7 ± 1.0	0.9 ± 0.7	2.1 ± 0.8			2					3				
20	173 426.2−323 759	10.4 ± 1.5	7.2 ± 1.2	5.4 ± 1.0	0.00 ± 0.14	−0.69 ± 0.24	1	1.5	16.9	15.4	14.9	1	1.5	12.8	12.1	11.9
21	173 427.2−323 422	9.3 ± 1.4	2.7 ± 1.0	2.0 ± 0.9	0.40 ± 0.16	−0.71 ± 0.18	1	5.4		17.1	16.1	1	5.5	13.5	12.7	12.4
22	173 428.6−323 337	2.1 ± 0.9	1.0 ± 0.6	2.3 ± 0.7			2					2				
23	173 430.3−323 605	6.2 ± 1.3	2.7 ± 0.8	2.9 ± 0.7	0.22 ± 0.18	≤−0.52	1	2.5		15.1	14.7	1	2.5	12.7	12.1	11.9
24	173 431.4−323 441	3.0 ± 0.9	0.8 ± 0.6	0.7 ± 0.6			1	4.3		17.1	16.3	1	4.6	14.1	13.4	(12.3)
25	173 431.8−323 326	17.0 ± 1.6	7.7 ± 1.2	8.0 ± 1.2	−0.11 ± 0.10	−0.42 ± 0.13	1	2.4		14.7	14.1	1	2.2	12.2	11.5	11.2
26	173 433.7−323 612	4.3 ± 1.1	1.6 ± 0.7				1	6.6		10.2	10.2	2				
27	173 434.7−323 350						1	4.2		10.3	10.3	3				
28	173 435.2−323 140	3.8 ± 0.9	2.1 ± 0.7	1.9 ± 0.6			0					1	5.4	(16.4)	14.3	12.9
29	173 435.8−323 548	11.3 ± 1.5	5.6 ± 1.1	5.0 ± 1.0	0.20 ± 0.13	−0.45 ± 0.15	1	1.6		17.3	16.7	3				
30	173 435.9−323 407						1	2.8		15.2	14.6	3				
31	173 436.9−322 737	6.0 ± 1.4	2.5 ± 0.9	3.5 ± 1.0	0.31 ± 0.21	−0.54 ± 0.28	1	0.8	16.2	15.0	14.5	2				
32	173 437.4−322 942	7.3 ± 1.3	4.1 ± 0.9	5.5 ± 1.0	−0.29 ± 0.17	−0.31 ± 0.31	1	2.7	14.2	13.1	12.8	2				
33	173 437.4−323 438	2.1 ± 1.6	1.4 ± 1.2	4.1 ± 1.3			2					2				
34	173 437.6−323 710	2.8 ± 1.0	2.4 ± 0.7	1.2 ± 0.6			1	4.2		17.6	17.0	3				
35	173 437.7−323 238	2.0 ± 0.9	1.4 ± 0.6	1.5 ± 0.6			1	0.7		17.5	16.8	1	0.9	14.3	13.5	13.3
36	173 438.7−323 512	7.3 ± 2.0		2.7 ± 1.4	0.47 ± 0.48	−0.60 ± 0.28	0					1	3.4	14.1	13.3	12.9
37	173 439.3−323 140	3.0 ± 0.8	0.5 ± 0.5	0.9 ± 0.6			1	6.2		15.5	15.0	3				

Table 1. continued.

#	XMMU J	pn	MOS1	MOS2	HR_1	HR_2	USNO (and GSC)					2MASS				
							Nr.	d	B	V	R	Nr.	d	J	H	K_S
		10^{-3} cts s^{-1}	10^{-3} cts s^{-1}	10^{-3} cts s^{-1}				($''$)					($''$)			
[1]	[2]	[3]	[4]	[5]	[6]	[7]	[8]	[9]	[10]	[11]	[12]	[13]	[14]	[15]	[16]	[17]
38	173 439.6−323 359	4.8 ± 1.9	3.9 ± 1.4	5.0 ± 1.2			1	6.7		13.2	13.2	4				
39	173 440.3−323 430	13.1 ± 3.3	8.4 ± 2.1	9.4 ± 2.4		≥0.40	1	1.2		14.8	14.0	1	0.9	12.4	11.8	11.6
40	173 441.3−323 554	5.9 ± 1.5	1.4 ± 0.9	2.4 ± 1.0	0.32 ± 0.36	−0.28 ± 0.25	1	7.0		16.7	16.2	3				
41	173 442.2−323 254	5.2 ± 1.4	1.7 ± 0.8	2.1 ± 0.8	−0.34 ± 0.29	−0.63 ± 0.63	1	4.9		17.6	16.7	4				
42	173 442.4−323 350	7.9 ± 2.0	2.8 ± 1.3	4.0 ± 1.3	0.16 ± 0.26	≤−0.47	1	3.9		14.3	14.1	1	4.3	12.6	11.8	11.2
43	173 442.5−323 043	2.1 ± 1.2	2.5 ± 0.8	2.5 ± 0.8			1	4.3	19.1	18.1	17.3	2				
44	173 442.5−323 455	1188.5 ± 13.0	519.5 ± 8.4	534.8 ± 8.2	−0.42 ± 0.01	−0.84 ± 0.01	1	1.8		5.71	5.73	1	1.7	5.53	5.52	5.54
45	173 443.9−323 851	3.8 ± 1.1	1.4 ± 0.7	1.2 ± 0.7			1	6.9	17.3	16.5	15.6	1	6.8	13.3	12.6	12.4
46	173 444.0−323 554	7.3 ± 1.5	2.3 ± 1.0	2.1 ± 1.6	−0.07 ± 0.29	0.14 ± 0.24	1	7.0		17.9	17.2	7				
47	173 444.2−323 710	6.3 ± 1.2	2.5 ± 0.8	1.3 ± 0.7	0.04 ± 0.21	≤−0.54	1	2.0		15.1	14.8	3				
48	173 444.2−323 632	2.3 ± 1.2	0.9 ± 0.7	3.0 ± 0.8			1	5.9			18.0	3				
49	173 444.8−323 047	2.6 ± 1.2	2.5 ± 0.8	2.7 ± 0.8			1	2.2	18.7	17.9	16.8	1	1.9	14.2	13.3	13.1
50	173 445.8−323 318	26.6 ± 2.3	15.6 ± 1.6	11.9 ± 1.5	0.64 ± 0.11	−0.17 ± 0.10	2					1	0.7	14.3	13.6	(13.8)
51	173 446.3−323 216	8.0 ± 1.4	3.0 ± 1.0	1.2 ± 0.8	0.01 ± 0.17	≤−0.65	1	5.9		15.2	14.9	2				
52	173447.1−323 558	4.1 ± 1.2		2.4 ± 0.9			1	3.0		16.9	15.8	3				
53	173 447.2−323 806	12.2 ± 1.6	5.1 ± 1.1	5.9 ± 1.0	0.22 ± 0.14	−0.46 ± 0.16	3					3				
54	173 447.8−324 108	13.1 ± 1.8	5.8 ± 1.2	5.8 ± 1.2	−0.70 ± 0.10	−0.48 ± 0.39	1	3.1	13.5	12.6	12.3	2				
55	173 448.1−323 422	21.9 ± 2.2	13.9 ± 1.5	11.4 ± 1.5	0.04 ± 0.11	−0.57 ± 0.11	1	2.0		13.4	13.2	1	1.9	11.7	11.2	11.0
56	173 448.1−323 520	15.2 ± 1.8	4.1 ± 1.2	5.0 ± 1.1	0.10 ± 0.13	−0.53 ± 0.13	1	2.2		11.2	11.2	3				
57	173 448.4−323 155	14.4 ± 1.7	8.0 ± 1.2	7.8 ± 1.2	0.01 ± 0.12	−0.48 ± 0.17	1	1.7		15.2	14.7	5				
58	173 449.4−324 351	3.5 ± 1.4	6.0 ± 1.4	2.6 ± 0.9			1	4.3	18.5	17.4	16.4	5				
59	173 449.5−324 548	2.2 ± 1.4	2.8 ± 1.1	3.5 ± 1.2			2					3				
60	173 450.5−323 806	2.4 ± 1.0	1.6 ± 0.7	1.9 ± 0.7			1	4.3		17.7	16.6	2				
61	173 450.5−323 938	2.9 ± 1.0	1.7 ± 0.7	1.4 ± 0.7			1	5.9	18.1	16.9	16.2	3				
62	173 450.7−323 356	1.4 ± 1.5	3.2 ± 1.0	3.1 ± 1.0			2					2				
63	173 451.1−323 520	11.8 ± 1.6	5.8 ± 1.1	5.7 ± 1.0	−0.04 ± 0.13	−0.71 ± 0.20	1	3.6		13.1	13.9	5				
64	173 451.5−323 310	8.9 ± 1.4	2.3 ± 0.8	2.2 ± 0.8	0.01 ± 0.17	−0.44 ± 0.21	1	1.5		15.8	15.4	2				
65	173 453.0−323 358	25.8 ± 2.1	11.4 ± 1.4	12.5 ± 1.4	0.06 ± 0.09	−0.60 ± 0.10	1	1.0		13.7	13.2	1	0.8	11.7	11.2	11.0
66	173 454.8−323 643	2.6 ± 0.9	1.8 ± 0.7	0.9 ± 0.7			1	7.0			17.1	2				
67	173 456.7−323 421	13.0 ± 1.7	4.9 ± 1.0	5.7 ± 1.0	−0.41 ± 0.12	−0.73 ± 0.27	1	2.7		14.0	13.8	3				
68	173 457.5−323 517	3.7 ± 1.1		2.8 ± 0.8			1	2.8		15.7	15.1	3				
69	173 457.9−323 631	5.6 ± 1.2	2.8 ± 0.7	3.2 ± 0.8	−0.11 ± 0.20	≤−0.49	1	2.1		16.9	16.4	1	2.0	14.3	13.4	13.0
70	173 500.6−323 422	14.1 ± 1.7	6.2 ± 1.1	8.1 ± 1.2	−0.08 ± 0.12	−0.45 ± 0.17	2					2				
71	173 505.3−323 433	6.8 ± 1.5	3.0 ± 0.9	3.9 ± 0.9	0.01 ± 0.20	−0.47 ± 0.28	1	6.9	15.2	14.3	13.9	1	6.7	12.4	11.9	11.7
72	173 507.9−322 905	4.2 ± 1.3	1.9 ± 0.9	2.1 ± 0.9			0					2				
73	173 517.4−323 548	3.2 ± 1.2	2.4 ± 0.8	1.2 ± 0.8			2					4				
74	173 520.5−323 410	5.6 ± 1.5	5.0 ± 1.1	3.0 ± 0.9	−0.47 ± 0.26	0.03 ± 0.45	1	1.7	17.9	16.5	15.9	4				
75	173 526.6−323 356	5.9 ± 1.7	1.0 ± 0.9		−0.25 ± 0.31	−0.01 ± 0.42	1	6.6	16.7	16.0	15.0	1	4.2	(12.8)	11.4	10.3
76	173 530.9−323 558	15.6 ± 2.3	7.5 ± 1.4	6.7 ± 1.5	≤−0.47	≥0.93	1	5.4		17.5	16.2	3				
77	173 531.5−323 512	2.5 ± 1.3	2.7 ± 1.0	1.6 ± 0.9			2					4				

No hardness ratio could be derived for source #39, since it lies inside the wings of the PSF of the bright central source HD 159 176 (#44).
IR magnitudes between brackets were flagged as uncertain in the 2MASS database because of band filling or diffraction spikes.